Using subtle variations in groundwater geochemistry to identify the proximity of individual geological structures: a case study from the Grimsel Test Site (Switzerland)

M. Stillings*, Z. K. Shipton, R. A. Lord and R. J. Lunn

Department of Civil and Environmental Engineering, University of Strathclyde, G1 1XJ, UK

MS, 0000-0001-8418-6866

* Correspondence: mark.stillings@strath.ac.uk

Abstract: Understanding groundwater flow and the evolution of groundwater chemistry in networks of fractures in crystalline rock is of fundamental interest for geothermal projects, nuclear waste disposal, and groundwater resources. Groundwater chemistry at a given location is typically conceived of being of a specific 'type' (e.g. meteoric, juvenile, connate, marine), with associated chemical types controlled through water–rock interactions. Minor chemical variations between groundwater sample locations with the same chemical type are generally considered as 'noise' in the geochemical data. Here, we argue that this noise contains useful information on the mineral phases encountered by the groundwater as it travels through specific flow pathways. We analyse the spatial variability of groundwater chemistry around the Grimsel Test Site (GTS), Switzerland, where groundwater is hosted in two lithologies: the Central Aar Granite and the Grimsel Granodiorite, where flow occurs predominantly in a fracture network created by brittle reactivation of ductile shear zones. Groundwater chemistry is analysed using principal component and hierarchical cluster analyses, which identify two groundwater types based on their chemistry. The primary control on groundwater type is the host rock lithology (granite/granodiorite). While the spatial variability of groundwater chemistry within each of the two lithologies is small, statistical analysis of the data shows similar groundwater chemistry in borehole intervals that are crosscut by similar geological structures, implying a structural control on groundwater chemistry. Our research shows that subtle chemical variations in groundwater provide information on fracture network connectivity and the proximity of geological features, that specific volumes of groundwater has interacted with.

Understanding how groundwater moves and chemically evolves in fractured crystalline rock is vital for many current and future subsurface engineering projects, such as the exploration of geothermal resources and the geological disposal of radioactive waste. Fractured rock networks can be complex, and hydraulic connectivity between intersecting fractures is variable, resulting in both well-connected and poorly connected areas of a single fracture network. Often a small percentage of fractures and faults can provide the main pathways for groundwater flow in crystalline systems (e.g. Evans *et al.* 2005) and even with borehole data, the predominant flow pathways are not always clear.

Groundwater geochemical investigations in fractured crystalline rock typically use major and minor dissolved ions and other geochemical analyses such as noble gases, and stable and radiogenic isotopes, to identify different groundwater bodies and characterize the groundwater system (Gerber *et al.* 2017; Fongoh *et al.* 2023). For example, dissolved ion chemistry, stable isotopes, and multivariate statistics can be applied to identify distinct stratified groundwater bodies hosted in fractured crystalline rock (Laaksoharju *et al.* 2008). In most cases, groundwater bodies are identified by significant changes in specific dissolved ions. For instance: increased carbonate is typical of limestone aquifers; increased sodium, calcium, chloride, and sulfate ion concentrations are typical of a shift to evaporite-rich aquifers (Wong *et al.* 2014). A standard statistical approach used to examine the variation of geochemical data sets is Principal Component Analysis (PCA) (Jolliffe 2002). PCA has successfully been applied to distinguish meteoric, glacial, marine, and brine endmember groundwaters, and

mixing between endmembers in a large geochemical dataset at Äspö hard rock laboratory in Sweden (Laaksoharju *et al.* 2008). PCA is readily used to identify different aquifer systems and recharge areas (Cloutier *et al.* 2008), aquifer-scale controls on hydrogeochemistry, and to identify groundwater facies (Belkhiri *et al.* 2011).

Here we hypothesize that different structural features, even when hosted in the same underlying lithology, may result in different water–rock chemical reactions occurring along the flow pathway due to variations in water residence times and mineralogical heterogeneities within structures. To test our hypothesis, we analyse groundwater chemical data collected from 11 borehole intervals that cut granite and granodiorite in the Grimsel Test Site, Switzerland (Stillings *et al.* 2021). We also classify the mineralogy of fractures, joints and dykes that cross-cut or are proximal to each interval. Using PCA, we show that whilst there are clearly identifiable differences in dissolved ion chemistry between the groundwater in the granite and the groundwater in the granodiorite, small but detectable changes *within* each lithology are also present. Comparing our geological observations with the groundwater chemical data, by a process of multiple staged multivariate analyses, we show that these variations in groundwater chemistry can be attributed to changes in fracture fill materials and to the proximity of mafic dykes in the rock volume surrounding each borehole sampling interval. Multiple staged multivariate analyses of groundwater chemical data could be a powerful prospecting tool for determining the mineralogical characteristics of local structures in the surrounding rock. This tool could be used to assess fracture connectivity, highlight pre-existing flow pathways and determine their proximity to specific geological features.

GTS geological setting

The Grimsel Test Site (GTS) is an underground rock laboratory containing a suite of groundwater monitoring boreholes. It is located in the upper Hasli valley, Canton of Bern, Switzerland (Fig. 1). The GTS is situated 200 to 600 m west of the Räterichsbodensee hydro-electric reservoir, at a depth of ~37 m below the reservoir water level (Fig. 1). A second connected hydro-dammed reservoir, Grimselsee, trends east–west ~500 m south of the GTS.

The GTS is hosted in calc-alkaline intrusions of the Central Aar Granite (CAGr) and Grimsel Granodiorite (GrGr) (Schaltegger 1990a, b, 1993) later cross-cut by metabasic dykes (Oberhansli et al. 1985) and later aplite dykes (Wehrens 2015). A gradual magmatic transition zone defined by 'schlieren' structures between the two lithologies implies a coeval emplacement (Schneeberger 2017; Schneeberger et al. 2019). The area underwent Alpine deformation at 20 Ma (Rolland et al. 2009), accommodated by ductile shear zones with later overprinting by cataclastic brittle deformation, often concentrated at lithological boundaries at the margin of the dykes (Schneeberger et al. 2019).

Previous observations of flow within the URL show that brittle fractures form the main conduits for groundwater flow at Grimsel (Schneeberger et al. 2018). The matrix porosity (%vol) of the crystalline granitoid host rock is 0.8–1.53% (Bossart et al. 1991). Fractures that host flow include joints formed by topographic exfoliation as a result of deglaciation (Ziegler et al. 2013, 2014), as well as fracturing related to the Alpine brittle reactivation of ductile shear zones. Geological lineament mapping (Fig. 1) at the surface above the GTS by (Schneeberger 2017; Schneeberger et al. 2017a) shows that laterally extensive zones of Alpine-associated brittle fracturing have trace lengths long enough that they likely extend from the surface to the GTS level. (Hoehn et al. 1998) note that flow in the GTS is fracture-dominated and they estimate an average hydraulic conductivity of 10–100 ms^{-1} from borehole data.

The CAGr and GrGr host rocks consist predominantly of quartz, potassium and plagioclase feldspar and micas, predominantly biotite (Schneeberger et al. 2019). The metabasic dykes consist predominantly of biotite, plagioclase, and potassium feldspar. Alpine-aged fissures (Alpine clefts) are filled with quartz, fluorite,
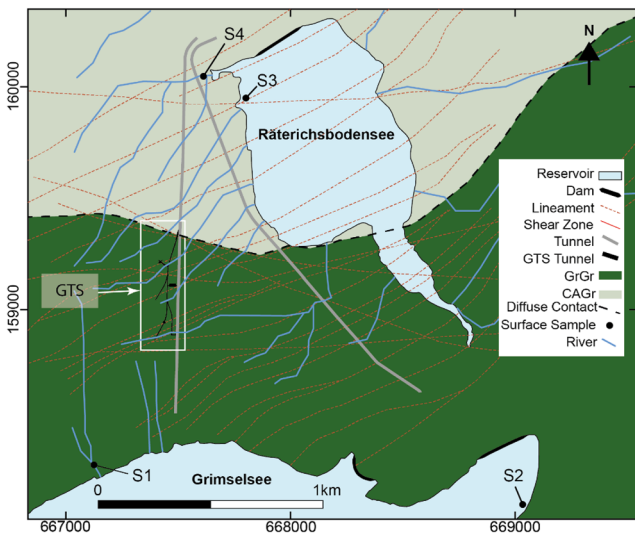
calcite (Cook 1998), and monazite minerals (Bergemann et al. 2017). The ductile shear zones entrain multiple different lithologies but are often localized along the metabasic dykes (Schneeberger et al. 2019).

Geological features at the GTS were mapped by Schneeberger (2017), through detailed structural geological observations and measurement of structure orientation and thickness along the tunnel walls of the GTS. Mapped shear zones and faults represent a brittle deformed volume of rock which can consist of several fractures. Often, where metabasic dykes have been fractured or sheared during faulting. Schneeberger et al. (2017a) produced detailed maps of the faults and shear zones which cut the tunnels and projected these into the surrounding rock mass, and where possible, confirming projections using borehole logs, images and cores. The thickness and orientation of metabasic dykes along the tunnel walls were also projected into the surrounding rock and matched against the borehole data. Figure 2a shows an amalgamated map, reproduced from separate fault and dyke maps (based
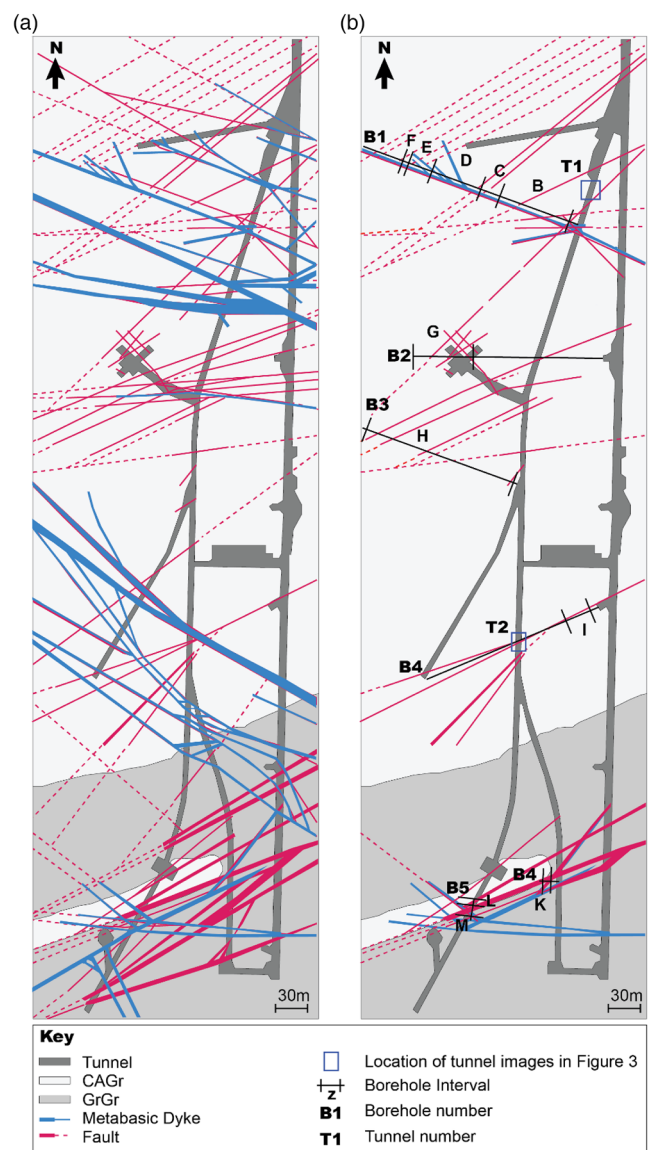

Fig. 1. Map of the Grimsel valley. Surface water sample sites (S1) river flowing into Grimselsee, (S2) Grimselsee, (S3) Räterichsbodensee, (S4) surface runoff into Räterichsbodensee. Faults in host rock lithology mapped from surface lineaments (red dashed lines) (Schneeberger 2017). Access tunnel (grey), Grimsel Test Site tunnels (black), and GTS area (white box). n.b. At the GTS scale, the transition between the two rock types is very diffuse. The position of this irregular, diffuse boundary at the surface (map) is not directly above the boundary at the tunnel level.

Fig. 2. (a) Petrographic map of the GTS based upon Schneeberger et al. (2017a) showing the two different host rock lithologies CAGr and GrGr, metabasic dykes (blue) and faults (pink). (b) Map of the boreholes (black line) sampled in this study (B1 to B5) and the sample intervals (B to M) overlain with the metabasic dykes (blue) and mapped faults (pink) that crosscut these intervals. Tunnel locations T1 and T2 (blue box) correspond to tunnel photographs in Figure 3.

on Schneeberger *et al.* 2017*a*), showing metabasic dykes overlain by faults. In most cases, brittle shearing along faults is localized along the metabasic dykes, and the granitic and metabasic dyke material has often been entrained into shear zones. The mapped faults (Fig. 2a) are composed of several fractures which form shear zones of varying thickness.

GTS hydrogeochemical setting

From isotopic analyses, groundwater sampled from boreholes in the GTS has been identified as meteoric (Schneeberger *et al.* 2017*b*) with values that correspond to the elevation of the ground surface above the GTS. Tritium and ^{14}C dating suggests groundwaters hosted within the GTS have residence times from 5 to 220 years (Keppler 1996; Schneeberger *et al.* 2017*b*, 2019). Chlorofluorocarbon analysis (CFCs) implies an apparent time of meteoric infiltration between 1947 and 1957, giving an apparent groundwater residence time from 65 to 75 years (Stillings *et al.* 2024), which is within the range of groundwater residence times indicated by the aforementioned tritium and ^{14}C tracing.

The meteoric groundwater sampled at the GTS is typical of dilute granitic waters; it has a low total dissolved solids (51.9–71.4 mg l^{-1}), is of a Na-Ca-TIC-F(SO_4) type composition and has a pH range from 8.13 to 9.78 (Schneeberger *et al.* 2017*b*; Stillings *et al.* 2021). Previous research has shown that the transition from CAGr in the north of the GTS to GrGr in the south correlates to an increase in the dissolved sodium, potassium, lithium and chloride concentrations and a decrease in the calcium ion concentration in (Schneeberger *et al.* 2017*b*).

Methods

To understand how structural geological features proximal to groundwater sample locations influence groundwater chemistry, groundwater samples for chemical analysis and structural observations have been recorded. Groundwater samples and structural geological observations were taken from 11 sampling intervals (B to M: Fig. 2b) from 5 boreholes (B1 to B5: Fig. 2b). These intervals were selected to cut different lithologies, fracture sets and fault rock types. Borehole intervals are at an elevation of ~1730 m above sea level, and the surface elevation above the boreholes varies from 2000 to 2200 m from north to south.

Structural feature data collection

For each of the 11 sampling intervals, structural geological data were compiled from Schneeberger *et al.*'s (2019) maps of metabasic dykes and faults (Fig. 2a) and from borehole core images (Fig. 3) where available. Core images existed in the GTS database for six of the borehole intervals **B**, **C**, **D**, **E**, **F** and **H** (Table 1) and were used to determine likely feature properties (e.g. fracture fill) for those features that directly intersected the borehole interval. For those intervals where borehole core images were unavailable (intervals **G**, **I**, **K**, **L**, and **M**), the maps by Schneeberger *et al.* (2019) (Fig. 2a) were used instead. These maps were developed by projecting geological observations taken from the tunnel wall. However, shear zones and metabasic dykes are not homogeneous – their width and fracture concentration vary along strike, even within the confines of the tunnel. As a consequence, the interpretation of cross-cutting structural features in intervals where the core images were not
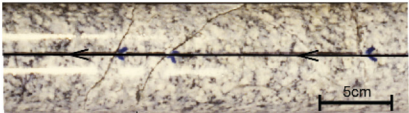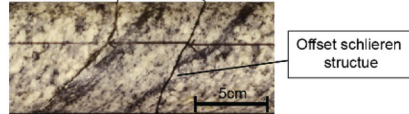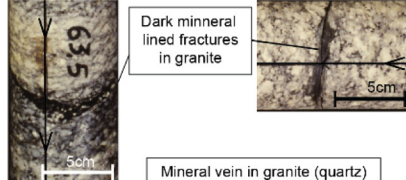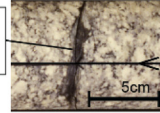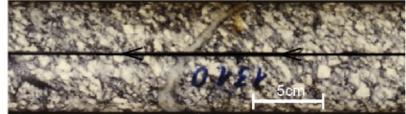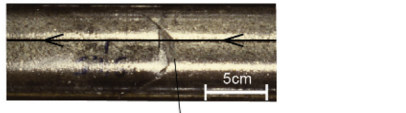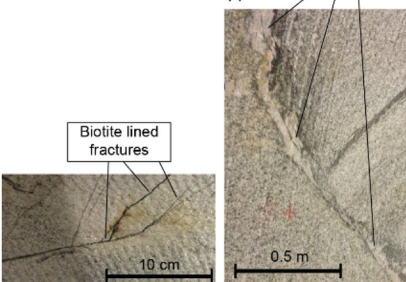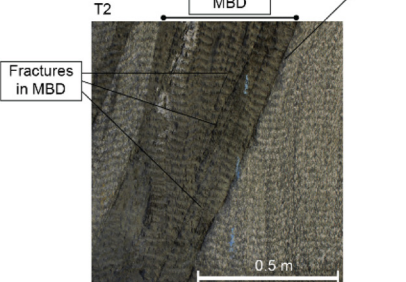

Fig. 3. Classification of fracture types: unlined fractures in granitic rock, lined fractures, fractures in metabasic dyke (MBD) from annotated core photographs and photographs of the GTS tunnel walls. Mineralogy from X-ray Diffraction (XRD) analysis compiled by Schneeberger *et al.* (2019).

available, are likely to be less accurate. Figure 2b shows a map of the structures that intersect, or are close to (<30 m), the 11 sampling intervals.

Based on observations from the tunnel walls and the core images, fractures that cross-cut the borehole intervals were classified into three types: (1) unlined fractures in granitic host rock, (2) fractures that have a lining of newly precipitated minerals on their walls (lined fractures), and (3) fractures in metabasic dykes. Figure 3 displays examples of these typical fracture types as expressed in the borehole images and on the tunnel walls. Unlined fractures in the granite and metabasic dykes are assumed to have mineralogies that correspond to the rocks that they cut. The mineralogy of lined fracture cannot be determined from the core images. However, lined fractures can contain precipitates of biotite/mica, epidote, or quartz. Shear fractures can also be lined with fault gouge, which will have less quartz and feldspar than the granitic host rocks and more micaceous minerals (biotite and muscovite) and clay minerals (Schneeberger *et al.* 2019).

Geochemical sampling and analysis

Groundwater samples were collected by Stillings *et al.* (2021) from Nov 2014 to Mar 2015 and Feb 2016 to Apr 2016 in the 11 sampling intervals (B to M: Fig. 2b). The boreholes were drilled between 1980 and 1998, and in all boreholes, packers were installed to enable groundwater sampling from specific isolated intervals. In total, 27 groundwater samples were collected per sample interval (methodology for sample collection analysis and associated groundwater dataset is available Stillings *et al.* 2021). Surface water samples were collected in August 2015 for this study. Locations were chosen based on site accessibility and to account for potential infiltration sources (Fig. 1). Samples were taken from Grimselsee (S2), Räterichsbodensee (S3), from glacial meltwater (S1) sampled from a stream higher up in the catchment above Grimselsee, which itself is recharged through the pump storage tunnel system, and from an ephemeral stream (S4) close to the bank of Räterichsbodensee (Fig. 1). Surface water sample collection and analysis followed the same procedure as the groundwater samples. Full methodological details are found in the supplementary information available from the University of Strathclyde KnowledgeBase at https://doi.org/10.15129/971b80a9-27b1-4dac-bbbb-b9aaf2051b65.

Statistical analysis

Principal Component Analysis (PCA) was used to identify the similarities and differences in water chemistry between sample locations. Statistical analysis of geochemical data was carried out using R (R Team 2018). PCA determines a set of orthogonal axes, or components (linear combinations of the relative concentrations of the measured dissolved ions), that explain the greatest variance within the data using the fewest components. The underlying similarity between samples can then be elucidated by displaying the samples as coordinates of the first two, most explanatory, principal components. Samples that plot at similar locations will contain similar relative combinations of dissolved ions.

Results

Structural geological observations at the groundwater sampling locations

Table 1 reports the cross-cutting features, as determined from the core images and the geological maps, for all borehole intervals. This includes the number of fractures of a given type for the 6 borehole intervals where core images were available, and any additional information regarding the quality of the core, visible mineral veins

Table 1. Structural geological observations from borehole core images and structural geological maps

Borehole interval	Category	Interval length (m)	Unlined fracture	Lined fracture	Fractures in MBD	Comments from borehole image/log	Intersecting features based on structural maps
B	Parallel to MBD cut by BSZ and MBD	40	45	13	5	15.9 and 32.5 m MBD not fractured, 51.4 m MBD and Qtz vein	1x BSZ zone, and parallel to 2x MBD
C	Parallel to MBD cut by BSZ	5	6	3	0		1x BSZ zone, and parallel to 2x MBD
D	Parallel to MBD cut by BSZ and MBD	29	75	26	37	63.5 m MBD fractured 10 cm, 76.5 m Qtz vein 10 cm, 78 m MBD fractured	1x BSZ zone, and parallel to 2x MBD
E	Parallel to MBD cut by BSZ and MBD	20	47	2	8		1x BSZ zone, and parallel to 2x MBD
F	Parallel to MBD and BSZ	2	8	1	0	112.34 m Rubble zone poor core recovery 10 cm long	No cross-cutting features on map, parallel to MBD
G	Cut by BSZ	-	-	-	-	No Borehole image/log available	3x BSZ
H	Cut by BZS and MBD	150	166	39	148	4 MBD sections cutting borehole	4x BSZ no mapped MBD
I	Parallel to BSZ	-	-	-	-	No cross-cutting features on map, parallel to BSZ
K	Cut by BSZ and MBD	-	-	-	-	No Borehole image/log available	1x BSZ shear zone and MBD
L	Cut by BSZ	-	-	-	-	No Borehole image/log available	1x BSZ
M	Cut by BSZ and MBD	-	-	-	-	No Borehole image/log available	4x BSZ and MBD

MBD, metabasic dyke; BSZ, brittle shear zone.

and observations of metabasic dykes. The mineral lining and fill type were difficult to determine with certainty based on visual inspection of the borehole core images. Therefore, filled/lined fractures are grouped into a single classification of 'lined fracture'.

All borehole intervals, except **F** and **I**, are intersected by brittle reactivated ductile shear zones (BSZs) (Fig. 2b, Table 1). Intervals **H** and **M** are cross-cut by 4 intersecting brittle shear zones and one of the brittle shear zones that intersects **M**, also cuts interval **K** (Fig. 2b). Interval **G**, hosted in the granite, has three cross-cutting brittle shear zones and is within one of the most densely fractured regions of the GTS containing multiple intersecting fracture sets.

Intervals **B**, **C**, **D**, and **E** are each intersected by one brittle reactivated ductile shear zone and run parallel to two metabasic dykes. **F**, located within the same borehole as **B**, **C**, **D** and **E**, has no mapped intersecting structures but does run parallel to a metabasic dyke and a brittle shear zone (which runs parallel to the dyke). Based on the maps (as core images are not available), interval **I** does not have any intersecting structural features, however the absence of fractures on the map (Fig. 2) does not necessarily indicate absence. Like **F**, interval **I** is parallel to a brittle shear zone. Sample location **I** sits in the magmatic transition zone between the Central Aar Granite in the north and the Grimsel Granodiorite in the south.

Fractures were counted (Table 1) in borehole intervals where core images or logs were available (**B**, **C**, **D**, **E**, **F**, and **H**). All of these intervals are cut by both open and lined fractures, however, only intervals **B**, **D**, **E** and **H** are cut by fractures within metabasic dykes. Intervals **C** and **F** are short (2 and 5 m, respectively) and contain mostly open fractures in the granitic rock. Intervals **B**, **D** and **E** are longer (20 to 40 m) and contain open fractures in both the granite and a metabasic dyke. Interval **H** is the longest sampling interval with available core image data (150 m); roughly half of the open fractures are within the granite in interval **H** and the other half cut a metabasic dyke (Table 1).

In summary, based on the mapped geological structures and borehole core images, the borehole intervals fall into four main categories in terms of their major cross-cutting structural features: (1) intervals cross-cut by one (or more) brittle shear zone within granitic rock; (2) intervals cross cut by one (or more) metabasic dyke; (3) intervals parallel to one (or more) brittle shear zone; (4) parallel to a metabasic dyke. Or fall into a combination of these categories. For example, interval **M** falls into categories 1 and 2 as it is cross-cut by both a brittle shear zone in granite and a metabasic dyke.

Water sample chemical results

Physiochemical results

Surface waters (reservoirs S2 and S4, glacial meltwater S1, and surface runoff S3) have near-neutral pH, and electrical conductivity (EC) ranges from 14–35 μScm^{-1} (Table 2). Groundwater is Na–Ca–TIC–F(SO$_4$) type, dilute and has a water temperature between 11.4°C and 17.3°C. Water temperature is generally higher in the south of the GTS than in the north (Table 2). The flow rate in each interval was recorded during sampling. Boreholes H and G have the highest flow rates, over 1×10^{-3} m^3 min^{-1}, while the other sampling intervals typically have flow rates less than 1×10^{-3} m^3 min^{-1}.

Groundwater electrical conductivity (EC) is higher than surface water conductivity, varying between 64.23 and 81.18 μS cm^{-1}. The average pH for each groundwater sampling interval ranges from 8.83 to 9.41. The spatial distribution of pH shows that samples from the north of the GTS (sample intervals B, C, D, E, F, G and H) typically have lower pH values of less than 9.0, while samples from the south of the GTS (sample intervals I, K, L, M) usually have pH values above 9.0.

Major and minor dissolved ions

Surface water and groundwater chemical data (Table 3) show that the lake water samples are marginally higher in Ca^{2+}, K$^+$, Mg^{2+}, Sr$^+$, SO$_4^{2-}$ and alkalinity compared to the river water samples. Dissolved Ca^{2+}, SO$_4^{2-}$ and Na$^+$ concentrations are lower in surface waters than in the groundwaters (Table 3).

The distribution of dissolved major ions indicates a difference in groundwater chemistry between the north and the south of the GTS. Table 3 shows the average major and minor dissolved ions across the sampled intervals. In agreement with previous findings (Schneeberger 2017), there is a higher concentration of Ca^{2+}, SO$_4^{2-}$ in the north, whereas Na$^+$, K$^+$, Li$^+$, and Cl$^-$ are higher in the south, associated with the transition from granite to granodiorite from north to south. Total alkalinity remains similar across the GTS, although groundwater pH is higher in the south. Analysis of the spatial distribution of dissolved ions indicates two main groups, reflected by relatively high (pH > 9.0) and low pH (pH < 9.0). Both show the same clear trends that separate the northern and southern groundwaters (previously reported in Schneeberger *et al.* 2017b). Dissolved sodium v. calcium and potassium v. calcium plots (Fig. 4) further highlight the general north–south spatial trend in groundwater chemistry. Groundwater samples from the north of the

Table 2. Host rock lithology and average values for temperature, conductivity and pH from all sampled groundwaters (*n* = 27, where *n* is the number of samples measured from each location) and values from individual surface waters

Sample location	Host rock lithology	Temp (°C)	EC (μScm^{-1})	pH	Eh (SHE) (mV)	Flow rate (L S^{-1})
B	CAGr	11.9	84.09	8.98	195.69	0.0029
C	CAGr	11.9	77.06	8.96	180.18	0.0028
D	CAGr	12.2	83.76	9.04	172.27	0.00755
E	CAGr	12.1	79.39	8.83	177.86	0.0056
F	CAGr	12.7	76.96	9.12	182.50	0.00168
G	CAGr	11.7	68.54	8.97	241.04	0.00427
H	CAGr	13.4	84.35	9.32	227.98	0.0115
I	CAGr	12.6	80.40	9.23	199.27	0.00772
K	GrGr	12.6	76.69	9.40	188.46	0.00422
L	GrGr	13.1	81.64	9.18	175.15	0.00277
M	GrGr	12.7	75.97	9.39	182.40	0.006
S1	River	11.2	16.70	6.67	117.40	-
S2	Lake	7.0	35.00	7.00	93.70	-
S3	River	8.1	14.70	6.85	55.60	-
S4	Lake	10.4	30.30	7.13	58.70	-

Boreholes are ordered from north to south.

Table 3. Major and minor dissolved ion chemistry for surface water sample, locations given in Figure 1

Location	CO₃ mg l⁻¹	HCO₃ mg l⁻¹	Al mg l⁻¹	Ca mg l⁻¹	Fe mg l⁻¹	K mg l⁻¹	Li mg l⁻¹	Mg mg l⁻¹	Mn mg l⁻¹	Na mg l⁻¹	Si mg l⁻¹	Sr mg l⁻¹	F mg l⁻¹	Cl mg l⁻¹	NO₃ mg l⁻¹	SO₄ mg l⁻¹
	5	5	0.001	0.05	0.001	0.09	0.001	0.001	0.001	0.05	0.01	0.01	0.10	0.10	0.10	0.10
S1	<5	<5	0.064	0.812	0.103	0.537	~	0.116	0.008	0.946	0.802	0.002	0.19	0.98	0.7	1.79
S2	<5	6	0.033	2.785	0.052	0.829	~	0.329	0.008	1.43	0.622	0.008	0.05	0.59	0.77	5.24
S3	<5	5	0.03	2.485	0.06	0.857	~	0.261	0.006	0.905	0.621	0.007	0.05	0.43	0.78	4.14
S4	<5	<5	0.042	0.711	0.05	0.273	~	0.084	0.002	0.056	0.771	0.003	0.04	0.04	0.57	0.65
B	<5	19	0.025	6.848	0.035	0.394	0.015	0.016	0.002	9.811	4.648	0.161	4.699	0.34	<0.1	7.07
C	<5	19	0.012	7.483	0.014	0.262	0.010	0.020	0.002	8.174	4.582	0.190	3.712	0.25	<0.1	6.61
D	<5	19	0.019	7.359	0.014	0.168	0.010	0.024	0.002	8.579	4.524	0.221	4.046	0.26	<0.1	6.16
E	<5	21	0.021	7.821	0.032	0.222	0.011	0.032	0.002	8.581	4.571	0.213	4.085	0.27	<0.1	6.21
F	<5	20	0.030	6.880	0.016	0.340	0.011	0.029	0.002	9.368	4.813	0.188	4.492	0.30	<0.1	6.09
G	<5	19	0.041	8.679	0.010	0.248	0.010	0.045	0.002	6.068	4.139	0.152	3.499	0.23	<0.1	6.44
H	<5	19	0.024	8.041	0.011	0.228	0.018	0.027	<0.001	8.568	4.414	0.143	4.392	0.67	<0.1	6.42
I	7	15	0.034	3.972	0.016	0.171	0.076	0.012	0.002	14.241	4.733	0.112	5.682	4.21	<0.1	4.27
K	6	17	0.062	5.213	0.029	0.477	0.038	0.040	0.002	10.949	4.730	0.164	4.332	1.84	<0.1	4.86
L	<5	20	0.032	6.456	0.079	0.405	0.035	0.042	0.004	10.857	3.157	0.173	5.324	1.81	<0.1	2.75
M	<5	19	0.024	5.310	0.011	0.468	0.033	0.021	<0.001	10.476	4.661	0.165	4.099	1.49	<0.1	4.94

Concentrations in mg l⁻¹. Quantification limit is given below each analyte. ~ **not measured.**

GTS have lower sodium and higher calcium concentrations (Fig. 4a). Groundwaters from the north of the GTS have lower potassium and higher calcium ion concentrations than the groundwaters hosted in the south. One exception is borehole I, sitting within the transition zone between CAGr and GrGr, which records a low potassium concentration but the highest sodium concentration.

Results of multivariate statistical analysis

Statistical analysis (PCA) was carried out on surface and groundwater dissolved ion chemistry data sets (Fig. 5a) to investigate the difference between groundwater and surface water chemistry. This was carried out in three stages so that major variations between different water bodies did not mask the more subtle variations between sampling interval locations in the same lithology. The first stage of PCA uses all water samples and shows that groundwaters are clustered together, with some variation, and that surface waters 'S' (white squares) are distinctly different from the groundwater samples. Ground and surface water samples shown are mainly separated by PC2. This reflects the finding that surface waters have higher concentrations of magnesium, manganese, and potassium, and groundwaters have higher concentrations of dissolved silica, sodium, and fluoride (see arrows on Fig. 5a for the direction of increase in each variable; the arrow length indicates the relative effect of a change in concentration). The increased silica and sodium are not surprising: sodium-silicate mineral dissolution from feldspars in granite is slow (Blum and Stillings 1995). Groundwaters with a residence time 5–220 years have a long time to equilibrate with the silicate granitic rock and thus have higher concentrations of dissolved silica than surface water.

Chemical variation within the groundwater can be further explored by removing the surface water and carrying out PCA analysis only on the groundwater dissolved ion chemical data (Fig. 5b). The PCA shows that groundwater sampling locations taken from the north of the GTS (B to H) cluster very close together on Figure 5b. However, there is a large variability between sampling locations in the south of the GTS (I, K, L and M) (Fig. 5b). In general, PC1 separates groundwater in the northern boreholes from the southern boreholes, the north has a higher concentration of calcium and strontium relative to sodium, chloride, lithium and fluoride. Schneeberger *et al.* (2017b) attributed the shift in calcium and sodium concentrations from the north to the south of the GTS to increased dissolution of albite into the matrix pore water in the granodiorite, and the precipitation of calcite and thus removal of calcium from the ground waters in the south (Schneeberger *et al.* 2017b).

To identify any intra-group variation within the northern groundwater sample locations, PCA was carried out on the data from boreholes B to H only (Fig. 5c). Three groundwater groups were identified from the analysis of the northern boreholes. Sample intervals C, D and E plot closely together forming a cluster with interval F plotting nearby. The variation of groundwater at location F from the main cluster (C, D and E) is explained by higher concentrations of dissolved sodium, strontium and silica compared to the other dissolved ions in F. Samples taken from B plot away from the main cluster and have higher concentrations of fluoride, sodium, silica, and chloride. Groundwaters from G and H plot in two distinct groups away from the main cluster of B, C, D, E and F. The separation from the main cluster (B to F) is due to increases in calcium, magnesium and aluminium in sample G and sulfate, chloride, and lithium in sample H (Fig. 5c).

Figure 5d shows a PCA carried out on only sample locations from the south of the GTS: I, K, L, and M (Fig. 5d). There is little chemical variation between groundwaters from locations K and M which plot close together. However, I and L plot separately and have lower concentrations of dissolved sulfate, potassium, silicon, and aluminium. The main chemical difference in I from the other groundwaters
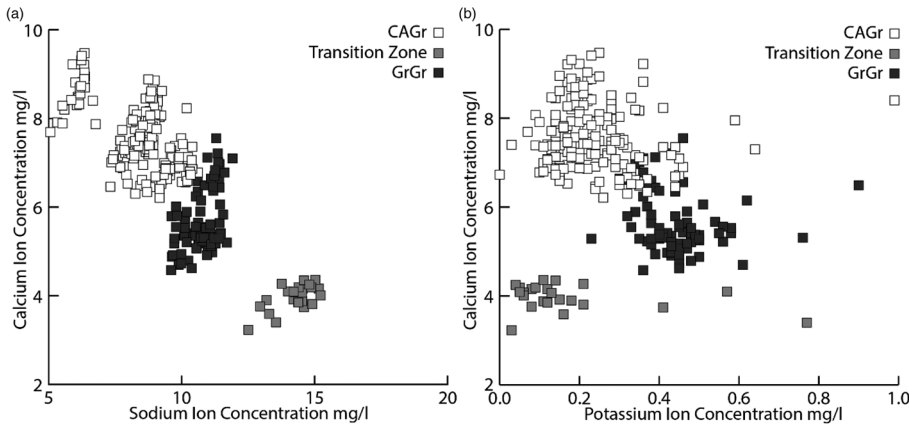
Fig. 4. (**a**) Sodium v. calcium and (**b**) potassium v. calcium ion groundwater concentrations for all groundwater sample locations at the GTS. Borehole intervals in the north of the GTS within the CAGr (white), south of the GTS in the GrGr (black), transition zone between CAGr and GrGr (grey) 3 results of multivariate statistical analysis.

is a higher concentration of sodium and lower concentrations of calcium and potassium, as is also visible in Figure 4. Borehole interval **I** also has higher concentrations of lithium and chloride compared with the other dissolved ions. Groundwater samples taken from **L** show higher concentrations of iron, calcium, and manganese.

To identify which groundwaters cluster together based on their dissolved ion chemistry we applied the hierarchical cluster analysis (HCA) non bias bootstrapping method outlined in Suzuki and Shimodaira (2006). This HCA method identifies significant clusters with statistical confidence limits that all samples within the cluster are similar and separate from the other cluster. Groundwaters with similar composition and relative concentrations of dissolved ions should sit within the same cluster. HCA was performed separately on the northern and southern groundwaters. HCA performed on the northern groundwater samples **B** to **H** is given in Figure 6a and shows that groundwaters hosted in boreholes **C**, **D**, **E** and **F** form a significant cluster (cluster 1), **H** and **B** form another cluster

(cluster 3), and **G** forms a separate cluster (cluster 2) all clusters have a greater than 95% confidence. Cluster analysis performed on the southern samples **I** to **M** gives four clusters with 85% confidence. Groundwater samples from location **I** form one cluster (cluster 3), and from **L** form another cluster (cluster 4). The other two clusters are composed of groundwaters from **K** and another cluster (cluster 1) which has samples from both **M** and **K** (cluster 2). Clusters 1 and 2 in the southern groundwaters (Fig. 6b) are each other's next nearest neighbour indicating that while they form different clusters, they are more similar to each other than the samples within clusters 3 and 4. This is not unsurprising, given groundwater samples from location K are split between clusters 1 and 2 (Fig. 6b).

Combining the geochemical and structural observations.

To investigate the controls on the variations in groundwater chemistry between boreholes hosted in a single lithology, i.e. in
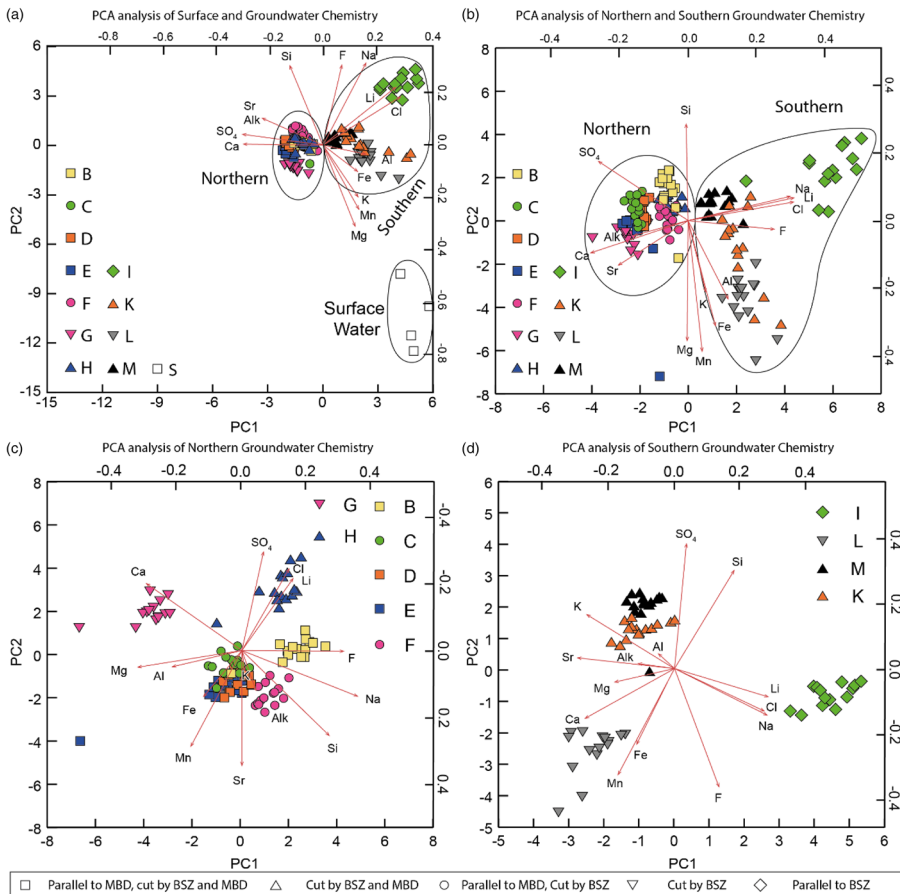

Fig. 5. PCA analysis of groundwater geochemical data, (**a**) all surface water and borehole geochemical data (surface water 'S'), (**b**) all borehole geochemical data from the GTS, (**c**) samples located in the north hosted in CAGr, (**d**) samples located in the south of the GTS hosted in GrGr. The legend at the bottom of the figures defines the symbol shape that represents the combination of structural features cutting an individual groundwater sample interval.
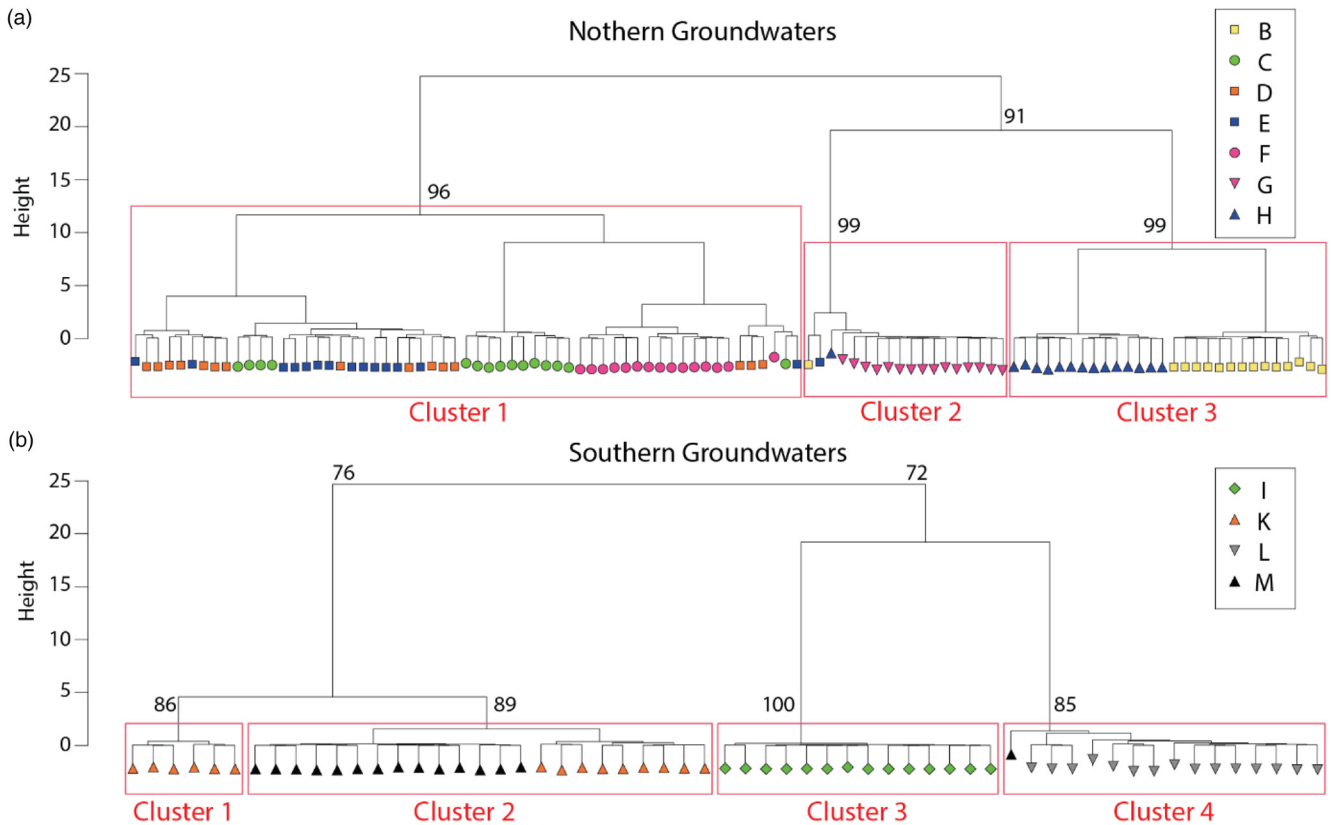
Fig. 6. Dendrogram based on HCA analysis of the northern (**a**) and southern (**b**) groundwater samples, clusters (red boxes) identified through approximately un-biased bootstrapping identifying 95% confidence in the northern groundwaters (**a**) and 85% confidence in the southern groundwaters (**b**).

either the north of the GTS (CAGr) or the south (GrGr) of the GTS, PCA analysis was carried out separately (Fig. 5c, d, respectively), and HCA analysis applied to identify significant clusters based on the geochemical data (Fig. 6a, b, respectively). Results were then compared with the mapped geological features and borehole fracture data (summarized in Table 1). If individual geological features affect the groundwater chemistry at a sampling location, there should be consistent commonalities between the cross-cutting geological features and the geochemical observations.

We find that locations with similar intersecting structures plot in similar locations in the PCA and form significant clusters. Locations **C**, **D**, **E** and **F**, in the north plot close to each other in Figure 5c form a significant cluster (Fig. 6a) and all have similar intersecting and nearby structures; they are cut by shear zones and are parallel to one MBD (Table 1) and in the case of **D** and **E** also crosscut by a MBD. Location **B** and **H** form a significant cluster and are both intersected by brittle shear zones and metabasic dykes (Table 1) and **B** also plots quite close to **C**, **D**, **E** and **F** but exhibits higher concentrations of sulfate, lithium, and chlorine (Fig. 5c). This could imply that groundwater flow is distributed differently between the fracture types in **B** and **H**, resulting in a slight change in the groundwater chemistry. Location **G** is separated from the other samples (Fig. 5c), forming its own significant cluster (Fig. 6a). **G** is only intersected by brittle shear zones (Table 1) with no nearby mapped dykes (Fig. 2). Location **G** has the lowest electrical conductivity and a lower total dissolved ion concentration than the other boreholes. Interval **G** is in a highly fractured region of the GTS where fracture surfaces in the shear zone may have different reactivities than other discontinuities. The very high flow rate in this interval reduces the groundwater residence time (Table 2). Shorter residence times will result in less time to reach chemical equilibrium between the groundwater and the fracture linings.

The sampling intervals in the south of the GTS are also separated by their groundwater chemistry in the PCA plot (Fig. 5d) and form

clusters. Locations **K** and **M** plot together and are cut by the same brittle shear zone and metabasic dyke (Table 1, Fig. 2b). They are separate from **L**, which is only cut by a brittle shear zone and **I**, which is parallel to a brittle shear zone (Table 1, Fig. 2b). **L** and **I** also form two separate clusters in the HCA analysis (Fig. 6b).

Discussion

Sample locations with a similar combination of crosscutting and proximal major structural features (brittle shear zones in granitic rock, metabasic dyke) appear to cluster on the PCA analysis (Fig. 5c, d) and form significant clusters (Fig. 6) based upon their groundwater dissolved ion chemistry. Given the two major structural features (brittle shear zones in granite and metabasic dykes) have different mineral assemblages (Fig. 3) then, does the difference in dissolved ion chemistry of these boreholes reflect the likely differences in mineral dissolution controlled by the cross cutting and nearby structures? Brittle shear zones in granite are composed of quartz, k-feldspar, and plagioclase and fractured metabasic dykes are mainly composed of biotite, plagioclase, and epidote. Groundwater-rock interaction with the granitic rock would increase the concentration of potassium, calcium, and sodium in the groundwater by hydrolysis reaction with the feldspar minerals present in the granite, thereby producing clay minerals as feldspars are hydrolysed (Oelkers and Schott 1995). Reactions with metabasic dykes will lead to hydrolysis of feldspar and biotite. When biotite undergoes hydrolysis clay is formed, and iron, potassium, fluoride and magnesium released into the groundwater (Kularatne and Pitawala 2012; Bray *et al.* 2014). Depending on the groundwater conditions (oxidizing/ reducing) iron may then undergo oxidation and be precipitated as hydrated iron oxide (Kularatne and Pitawala 2012), or react with sulfide and precipitate as pyrite thereby reducing the concentration of iron in the groundwater. As plagioclase is present within the metabasic dykes there would also be an increase in sodium

and calcium as the plagioclase is hydrolysed with the Na/Ca ratio reflecting the plagioclase mineralogy present (Banks and Frengstad 2006). One further control which could affect the dissolved ion concentration, and thus account for the location-to-location variation in the groundwater chemistry, is a variability in the chemical composition of the source water between sampling locations. Previously published isotopic analysis shows that all groundwaters sampled from boreholes in the GTS reflect a meteoric water source (Schneeberger *et al.* 2017*b*). The PCA analysis (Fig. 5a) indicates that the different meteoric water sources (river, runoff and reservoir water) have similar dissolved ion chemistries. Thus, the observed variations in groundwater dissolved ion chemistry at depth, most likely evolve through water–rock interactions in the fracture system during transport from the surface to the sampling locations at depth in the GTS.

In the north of the GTS in the CAGr, location **G** is the only interval which is crosscut by only brittle shear zones. Groundwater in interval **G** differs slightly from the rest of the northern groundwaters, forming a cluster (Fig. 6a), with higher calcium relative to other dissolved ions. Higher calcium can be attributed to water–rock interaction within fractures in the CAGr which has been previously attributed to increased groundwater calcium concentration at the GTS (Schneeberger *et al.* 2017*b*). Borehole intervals **B**, **C**, **D**, **E**, **F** and **H** are all cut by brittle shear zones and are cut by, or run parallel to, metabasic dykes. Their groundwater chemistries are very similar, with the exceptions of **H** and **B** which have slight differences in dissolved ion concentration (Fig. 5c). The influence of metabasic dykes would increase the concentrations of dissolved iron, magnesium and aluminium in the ground water as biotite in the dykes becomes hydrolysed. The groundwaters in intervals **B** and **H** have slightly higher concentrations of sodium, lithium and calcium and lower concentrations of dissolved ions associated with metabasic dykes and are therefore likely fed by a combination of fractures cutting the granite (lined or unlined) and metabasic dykes leading to variabilities in their geochemistry in comparison to **C**, **D**, **E** and **F**. **C**, **D** and **E** have higher iron, magnesium and aluminium relative to other ions indicating an influence from water–rock reaction with metabasic dykes, as biotite is hydrolysed and iron and magnesium released. The data indicates that groundwaters feeding **C**, **D** and **E** likely flow through a higher proportion of fractures within the metabasic dykes compared with the other boreholes in the north of the GTS. In the north of the GTS the differences in dissolved ion chemistry between borehole intervals highlighted through PCA and statistically clustered using HCA analysis shows feasible differences in groundwater chemistry which can be related to the water-mineral reactions with the proximal flow bearing structures to the borehole sample intervals.

In the south of the GTS, borehole intervals **K** and **M** are both intersected by the same brittle shear zone and metabasic dyke, and the groundwater chemistry in these boreholes plots in the same area of the PCA (Fig. 5d). The similar groundwater chemistry and likely connected flow pathways in **K** and **M** implies the minerals lining the flow pathways are similar and interact with minerals associated with the metabasic dyke (biotite, muscovite and plagioclase) and GrGr. Low sodium and calcium compared with the other southern samples indicate a lack of interaction with feldspathic minerals and increased potassium from biotite and muscovite hydrolysis in the metabasic dykes. Interval **L**, hosted in GrGr and cut by a brittle shear zone, has increased concentrations of iron and calcium perhaps indicating a higher proportion of biotite lining the fractures and unlined fractures in the GrGr that has a high calcium feldspar content. Interval **I** sits in the transition zone between CAGr and GrGr, adjacent to a brittle reactivated shear zone. Borehole **I** has a higher sodium and lithium concentrations and lower potassium and calcium concentrations than **K**, **L** and **M**. It is likely that Na-feldspar, typically found in the granite, is more dominant in the fractures feeding **I**.

Investigating the differences in groundwater chemistry using a staged PCA approach where each grouping of sample locations was further examined by a subsequent round of PCA allows the inter- and intra- group variance to be identified and examined. In this case, the main variance in groundwater chemistry between all the boreholes in the GTS, as identified by the PCA analysis, was consistent with previous groundwater chemical investigations (Schneeberger *et al.* 2017*b*). However, by applying a further level of PCA analysis and analysing each progressive cluster separately, the variance in groundwater chemistry within each lithology becomes apparent. We show a relationship between the different cross-cutting geological structures, or the absence thereof, and the subtle variations observed in the groundwater chemistry. These variations can be explained by alteration, dissolution and precipitation of the predominant minerals that characterize each structure. With further research, this staged PCA approach could prove useful as a site investigation tool. Subtle changes in groundwater chemistry could provide evidence of nearby structural or mineralogical features, even when they do not crosscut the borehole. Understanding subsurface interconnectivity is crucial for successful geothermal energy schemes to maintain yields and ensure resource sustainability (Philipp *et al.* 2007; Liu *et al.* 2023). Using the subtle variations in the geochemical data to understand subsurface interconnectivity and the relationship to geological structures could provide valuable information for subsurface engineering projects, such as geothermal energy exploration, where faults and fractured shear zones can be the main permeable conduits for hot water.

References

Banks, D. and Frengstad, B. 2006. Evolution of groundwater chemical composition by plagioclase hydrolysis in Norwegian anorthosites. *Geochimica et Cosmochimica Acta*, **70**, 1337–1355, https://doi.org/10.1016/j.gca.2005.11.025

Belkhiri, L., Boudoukha, A. and Mouni, L. 2011. A multivariate statistical analysis of groundwater chemistry data. *International Journal of Environmental Research*, **5**, 537–544.

Bergemann, C., Gnos, E. *et al.* 2017. Th-Pb ion probe dating of zoned hydrothermal monazite and its implications for repeated shear zone activity: an example from the Central Alps, Switzerland. *Tectonics*, **36**, 671–689, https://doi.org/10.1002/2016TC004407

Blum, A.E. and Stillings, L.L. 1995. Chapter 7. Feldspar dissolution kinetics. *In:* White, A.F. and Brantley, S.L. (eds) *Chemical Weathering Rates of Silicate*

Minerals. De Gruyter, Berlin, Boston, 291–352, https://doi.org/10.1515/9781501509650-009

Bossart, P., Mazurek, M., Hellmuth, K.H., Siitari-Kauppi, M. and Schneebeli, M. 1991. *Grimsel Test Site: Structural Geology and Water Flow-Paths in the Migration Shear-Zone*. **NAGRA-NTB–91-12**.

Bray, A.W., Benning, L.G., Bonneville, S. and Oelkers, E.H. 2014. Biotite surface chemistry as a function of aqueous fluid composition. *Geochimica et Cosmochimica Acta*, **128**, 58–70, https://doi.org/10.1016/j.gca.2013.12.002

Cloutier, V., Lefebvre, R., Therrien, R. and Savard, M.M. 2008. Multivariate statistical analysis of geochemical data as indicative of the hydrogeochemical evolution of groundwater in a sedimentary rock aquifer system. *Journal of Hydrology*, **353**, 294–313, https://doi.org/10.1016/j.jhydrol.2008.02.015

Cook, R.B. 1998. Fluorite on Quartz Chamonix, Haute-Savoie, France. *Rocks & Minerals*, **73**, 54–56, https://doi.org/10.1080/00357529809603062

Evans, K.F., Genter, A. and Sausse, J. 2005. Permeability creation and damage due to massive fluid injections into granite at 3.5 km at Soultz: 1. Borehole observations. *Journal of Geophysical Research: Solid Earth*, **110**, https://doi.org/10.1029/2004JB003169

Fongoh, E.J., Celle, H. *et al.* 2023. Multitracer approach towards an improved understanding of shallow hard rock aquifers and a more sustainable groundwater management, case of Yaounde, Cameroon. *Environmental Earth Sciences*, **82**, https://doi.org/10.1007/s12665-023-10783-9

Gerber, C., Vaikmäe, R. *et al.* 2017. Using 81Kr and noble gases to characterize and date groundwater and brines in the Baltic Artesian Basin on the one-million-year timescale. *Geochimica et Cosmochimica Acta*, **205**, 187–210, https://doi.org/10.1016/j.gca.2017.01.033

Hoehn, E., Eikenberg, J., Fierz, T., Drost, W. and Reichlmayr, E. 1998. The Grimsel Migration Experiment: field injection-withdrawal experiments in fractured rock with sorbing tracers. *Journal of Contaminant Hydrology*, **34**, 85–106, https://doi.org/10.1016/S0169-7722(98)00083-7

Jolliffe, I.T. 2002. Principal component analysis for special types of data. *In: Principal Component Analysis*. Springer, New York, NY, 338–372, https://doi.org/10.1007/0-387-22440-8_13

Keppler, A. 1996. *Hydrogeologische, hydrochemische und isotopenhydrologische Untersuchungen an den Oberflächen- und Kluftwässern im Grimselgebiet, Schweiz*.

Kularatne, K. and Pitawala, H. 2012. Leaching of fluoride from biotite mica in soil: implications for fluoride in shallow groundwater. *International Scholarly Research Notices*, **2012**

Laaksoharju, M., Gascoyne, M. and Gurban, I. 2008. Understanding groundwater chemistry using mixing models. *Applied Geochemistry*, **23**, 1921–1940, https://doi.org/10.1016/j.apgeochem.2008.02.018

Liu, G., Yuan, Z., Zhou, C., Fu, Z., Rao, Z. and Liao, S. 2023. Heat extraction of enhanced geothermal system: impacts of fracture topological complexities. *Applied Thermal Engineering*, **219**, 119236, https://doi.org/10.1016/j.applthermaleng.2022.119236

Oberhansli, R., Hunziker, J.C., Martinotti, G. and Stern, W.B. 1985. Geochemistry, geochronology and petrology of monte mucrone - an example of eo-alpine eclogitization of permian granitoides in the Sesia-Lanzo Zone, Western Alps, Italy. *Chemical Geology*, **52**, 165–184.

Oelkers, E.H. and Schott, J. 1995. Experimental study of anorthite dissolution and the relative mechanism of feldspar hydrolysis. *Geochimica et Cosmochimica Acta*, **59**, 5039–5053, https://doi.org/10.1016/0016-7037(95)00326-6

Philipp, S.L., Gudmundsson, A. and Oelrich, A.R.I. 2007. How structural geology can contribute to make geothermal projects successful. European Geothermal Congress, Unterhaching, Germany, **30**.

Rolland, Y., Cox, S.F. and Corsini, M. 2009. Constraining deformation stages in brittle-ductile shear zones from combined field mapping and 40Ar/39Ar dating: the structural evolution of the Grimsel Pass area (Aar Massif, Swiss Alps). *Journal of Structural Geology*, **31**, 1377–1394, https://doi.org/10.1016/j.jsg.2009.08.003

R Team 2018. *R: A Language and Environment for Statistical Computing*. R Foundation for Statistical Computing, Vienna, https://www.r-project.org

Schaltegger, U. 1990*a*. The central Aar Granite - highly differentiated calc-alkaline magmatism in the Aar Massif (Central Alps, Switzerland). *European Journal of Mineralogy*, **2**, 245–259, https://doi.org/10.1127/ejm/2/2/0245

Schaltegger, U. 1990*b*. Postmagmatic resetting of Rb-Sr whole rock ages - a study in the central Aar Granite (Central Alps, Switzerland). *Geologische Rundschau*, **79**, 709–724, https://doi.org/10.1007/BF01879210

Schaltegger, U. 1993. The evolution of the polymetamorphic basement in the central alps unraveled by precise U-Pb zircon dating. *Contributions to Mineralogy and Petrology*, **113**, 466–478, https://doi.org/10.1007/BF00698316

Schneeberger, R. 2017. *Interplay in 3D Between Faults and Water Flow Paths in Crystalline Bedrock (Grimsel, Switzerland)*. PhD, University of Bern.

Schneeberger, R., De La Varga, M., Egli, D., Berger, A., Kober, F., Wellmann, F. and Herwegh, M. 2017*a*. Methods and uncertainty estimations of 3-D structural modelling in crystalline rocks: a case study. *Solid Earth*, **8**, 987–1002, https://doi.org/10.5194/se-8-987-2017

Schneeberger, R., Mader, U.K. and Waber, H.N. 2017*b*. Hydrochemical and isotopic (delta H-2, delta O-18, H-3) characterization of fracture water in crystalline rock (Grimsel, Switzerland). 15th Water-Rock Interaction International Symposium, Evora, Portugal, Wri-15, **17**, 738–741.

Schneeberger, R., Egli, D., Lanyon, G.W., Mäder, U.K., Berger, A., Kober, F. and Herwegh, M. 2018. Structural-permeability favorability in crystalline rocks and implications for groundwater flow paths: a case study from the Aar Massif (central Switzerland). *Hydrogeology Journal*, **26**, 2725–2738, https://doi.org/10.1007/s10040-018-1826-y

Schneeberger, R., Kober, F., Lanyon, G.W., Mäder, U.K., Spillmann, T. and Blechschmid, I. 2019. *Grimsel Test Site: Revisiting the Site-Specific Geoscientific Knowledge*. Technical Report **19-01**. NAGRA.

Stillings, M., Lunn, R.J., Pytharouli, S., Shipton, Z.K., Kinali, M., Lord, R. and Thompson, S. 2021. Microseismic events cause significant pH drops in groundwater. *Geophysical Research Letters*, **48**, https://doi.org/10.1029/2020GL089885

Stillings, M., Lunn, R.J., Shipton, Z.K., Lord, R.A.,Thompson, S. and Knapp, M. 2024. Fingerprinting dissolved organic compounds: a potential tool for identifying the surface infiltration environments of meteoric groundwaters. *Geoenergy*, **2**, https://doi.org/10.1144/geoenergy2023-036

Suzuki, R. and Shimodaira, H. 2006. Pvclust: an R package for assessing the uncertainty in hierarchical clustering. *Bioinformatics*, **22(12)**, 1540–1542, https://doi.org/10.1093/bioinformatics/btl117

Wehrens, P. 2015. *Structural Evolution in the Aar Massif (Haslital Transect): Implications for Midcrustal Deformation*. University of Bern, Switzerland.

Wong, C.I., Kromann, J.S., Hunt, B.B., Smith, B.A. and Banner, J.L. 2014. Investigating groundwater flow between Edwards and Trinity Aquifers in Central Texas. *Groundwater*, **52**, 624–639, https://doi.org/10.1111/gwat.12106

Ziegler, M., Loew, S. and Moore, J.R. 2013. Distribution and inferred age of exfoliation joints in the Aar Granite of the central Swiss Alps and relationship to Quaternary landscape evolution. *Geomorphology*, **201**, 344–362, https://doi.org/10.1016/j.geomorph.2013.07.010

Ziegler, M., Loew, S. and Bahat, D. 2014. Growth of exfoliation joints and near-surface stress orientations inferred from fractographic markings observed in the upper Aar valley (Swiss Alps). *Tectonophysics*, **626**, 1–20, https://doi.org/10.1016/j.tecto.2014.03.017